Wet Air Oxidation of Formic Acid Using Nanoparticle-Modified Polysulfone Hollow Fibers as Gas–Liquid Contactors

Seth R. Hogg,[†] Satish Muthu,[‡] Michael O'Callaghan,[†] Jean-Francois Lahitte,[§,⊥] and Merlin L. Bruening*[,†]

[†]Department of Chemistry, Michigan State University, East Lansing, Michigan 48824

[‡]Department of Chemical Engineering and Materials Science, Michigan State University, East Lansing, Michigan 48824

[§]INPT, UPS, Laboratoire de Génie Chimique, Université de Toulouse, 118 Route de Narbonne, F-31062 Toulouse, France

[⊥]Laboratoire de Génie Chimique, CNRS, F-31030 Toulouse, France

ABSTRACT: Catalytic wet air oxidation (CWAO) using membrane contactors is attractive for remediation of aqueous pollutants, but previous studies of even simple reactions such as formic acid oxidation required multiple passes through tubular ceramic membrane contactors to achieve high conversion. This work aims to increase single-pass CWAO conversions by using polysulfone (PS) hollow fibers as contactors to reduce diffusion distances in the fiber lumen. Alternating adsorption of polycations and citrate-stabilized platinum colloids in fiber walls provides catalytically active PS hollow fibers. Using a single PS fiber, 50% oxidation of a 50 mM formic acid feed solution results from a single pass through the fiber lumen (15 cm length) with a solution residence time of 40 s. Increasing the number of PS fibers to five while maintaining the same volumetric flow rate leads to over 90% oxidation, suggesting that further scale up in the number of fibers will facilitate high single pass conversions at increased flow rates. The high conversion compared to prior studies with ceramic fibers stems from shorter diffusion distances in the fiber lumen. However, the activity of the Pt catalyst is 20-fold lower than in previous ceramic fibers. Focusing the Pt deposition near the fiber lumen and limiting pore wetting to this region might increase the activity of the catalyst.

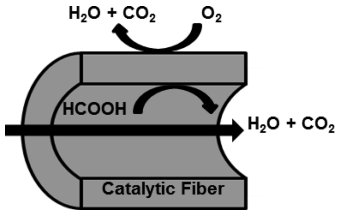

KEYWORDS: *layer-by-layer (LBL), Pt nanoparticles, wet air oxidation, hollow fiber membranes, catalytic membrane reactors, formic acid oxidation, gas-liquid contactor*

1. INTRODUCTION

Catalytic wet air oxidation (CWAO) is potentially attractive for remediating aqueous streams containing organic pollutants that are too dilute for efficient incineration and too concentrated for biological processing.[1,2] Because of the low solubility of O_2 in water, however, CWAO requires high air pressures to achieve appreciable oxidation. Gas-liquid membrane contactors control the introduction of multiple reactants to a fixed catalyst surface[3,4] and can potentially overcome O_2-solubility limitations to provide higher CWAO conversions than conventional batch reactors operating under similar gas pressures.[5] Such contactors utilize membrane pores to create an interface between liquid and gas streams (Figure 1), and management of the gas overpressure in these systems can sometimes control the degree of pore wetting to position the gas–liquid interface near an area rich in catalyst.[6] In specific cases, the increased availability of gaseous reactant at the catalyst surface gives conversion rates three to six times higher in membrane contactors than in trickle bed reactors.[2,5] Hollow fiber membranes provide an attractive choice for contactor systems because of their large surface-area-to-volume ratio and high packing density,[4,7−10] and several recent studies employed catalytic hollow fibers as membrane reactors.[11−17] This work examines whether immobilization of nanoparticle catalysts in polymeric hollow fibers enhances the oxidation of a model pollutant compared to oxidation in ceramic fibers with much larger diameters. The small lumen diameter in the polymeric fibers should greatly reduce diffusion distances to increase pollutant conversion relative to typical ceramic fibers with much larger inner diameters.

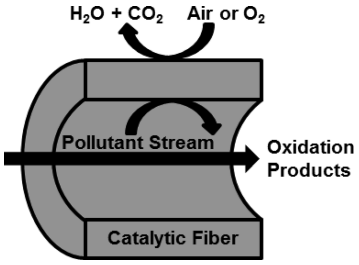

Figure 1. Schematic drawing of a cylindrical membrane contactor for CWAO with liquid feed passing through the lumen and gas supplied to the shell side.[18]

Metal nanoparticles are promising catalysts for hollow fiber membrane contactors because of their high surface area to mass ratio.[19−27] Additionally, nanoparticles often possess unusual electronic and catalytic properties that stem from their unique

size between the bulk and molecular regimes.[19,20,28] Entrapment of such nanoparticles in a hollow fiber both prevents catalyst aggregation and allows for continuous reactions. Although several methods exist for forming nanoparticles by reduction of metal ions in membranes,[18,29,30] synthesis of nanoparticles in solution prior to loading onto supports typically yields more uniform particle shapes and diameters.[22,29,31−38] However, loading of preformed nanoparticles in membranes requires strong adhesion between the nanoparticle and the support.

We employ layer-by-layer (LBL) adsorption of nanoparticles and oppositely charged polyelectrolytes to immobilize preformed catalytic nanoparticles in membrane pores.[39−45] LBL deposition occurs on many substrate materials with geometries that include flat surfaces, membrane pores, cylindrical particles, and carbon nanotubes.[18,35,36,38,39,46,47] Thus, this technique is amenable to hollow-fiber modification. Moreover, the amount of immobilized particles increases with the number of adsorbed layers.

Miachon and coworkers examined tubular ceramic membranes as interfacial contactors for CWAO and found increased activity compared to a stirred tank reactor because of control over the position of the gas-liquid interface within the membrane.[5,48−52] Notably, LBL deposition of polyelectrolyte multilayers and Pt nanoparticles yielded a membrane reactor with the highest Pt activity among those tested.[18] However, the pollutant conversion was relatively low, and the price of the ceramic membranes might limit their potential application.[53] Polymeric hollow fibers may provide a much less expensive option for CWAO of organic pollutants if these membranes are sufficiently stable.

This paper describes LBL deposition of polyelectrolytes and citrate-stabilized Pt nanoparticles in polysulfone (PS) hollow fibers to create membrane reactors for CWAO of aqueous formic acid. We compare catalytic activities and conversions to previous work with ceramic hollow fiber membranes and model concentration profiles in membrane reactors to assess the potential benefits of the polymeric hollow fibers. The small diameters of these fibers give rise to higher single-pass conversions compared to previous, larger ceramic membranes, but catalyst activity is more modest in the polymeric hollow fibers.

2. EXPERIMENTAL SECTION

2.1. Materials. Poly(sodium 4-styrenesulfonate) (PSS, M_w = 70 000 Da), branched polyethyleneimine (PEI, M_w = 25 000 Da), hexachloroplatinic acid hexahydrate, sodium chloride, and sodium citrate were used as received from Sigma-Aldrich. Formic acid from Mallinckrodt Baker and compressed O_2 (industrial purity, 99.5%) from Airgas were also used as received. Deionized water (Milli-Q purification system, 18.2 MΩ cm) was used for rinsing the membranes and preparation of the polyelectrolyte and formic acid solutions. The pH values of the polyelectrolyte solutions were adjusted with dilute solutions of HCl and NaOH.

A PS microfiltration hollow fiber membrane module containing 270 fibers was obtained from GE Lifesciences (model CFP-6-D-6A). Individual fibers were removed from the module and repotted in 15 cm lengths. Membranes have a stated maximum pore size of 650 nm, an inner diameter of 750 μm, and a wall thickness of 225 μm.

2.2. Synthesis of Citrate-Stabilized Pt Nanoparticles. Synthesis of Pt nanoparticles followed a literature procedure that uses citrate to both reduce the Pt and prevent particle aggregation through charge repulsion.[54] Forty mg of platinic acid dissolved in 255 mL water was stirred and heated to reflux in a 500 mL round bottom flask before addition of 30 mL of a 1% (w/w) sodium citrate solution. The Pt solution slowly darkened from amber to brown and eventually to black during 4 h of reflux. After cooling to room temperature, the Pt colloid solution was stored in an amber glass bottle in a refrigerator. Immediately prior to deposition, the Pt colloids were diluted 12.5:1 with deionized water. Our previous transmission electron microscopy images of Pt nanoparticles prepared using this method showed a size distribution centered around 3 nm.[18]

2.3. Modification of Hollow Fiber Membranes. Following a literature procedure, a 1.3 cm diameter PVC tube housed the hollow fibers potted in epoxy resin (Loctite E-00NS Hysol Epoxy Adhesive).[55] Modules contained either one centered fiber or five fibers arranged in an X geometry with fiber lengths of 15 cm between the epoxy resin at each end. Immediately prior to introduction into the module, all deposition solutions passed through a fresh filter (Ahlstrom 2.5 μm qualitative filter paper) to remove any particles that might block fiber pores. The polyelectrolyte solutions contained either 0.8 mM PSS or 0.8 mM PEI along with 20 mM NaCl. (Polymer concentrations are with respect to the repeating unit.) Initially, the PS hollow fibers were rinsed with distilled water for 30 min in a dead end setup with water flowing from shell to lumen. During polyelectrolyte and nanoparticle adsorption, solutions passed from the lumen to the shell side using lumen cross-flow under an applied pressure of 0.34 bar. A partially closed valve at the lumen exit forced most of the flow through the membrane pores (Figure 2). Modification began by

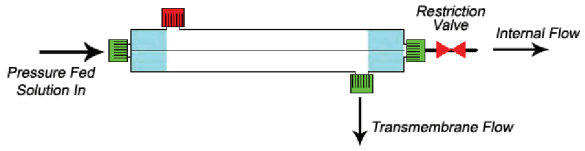

Figure 2. Apparatus for fiber modification with polyelectrolyte multilayers. Deposition solutions enter the fiber lumen before exiting under cross-flow. A valve located at the lumen exit creates backpressure to force most solution through the high surface area pores to the shell. Rinsing after depositions proceeds through passage of water from the shell side through the lumen in a dead-end setup.

passage of 250 mL of PSS solution through the fiber to adsorb PSS via hydrophobic interactions with PS.[56,57] A deionized water rinse from shell through lumen (until the conductivity of the permeate was less than 10 μS, 100−800 mL of rinsing) removed excess polyelectrolyte from the membrane. Next, passage of 250 mL of PEI solution through the membrane followed by rinsing completed deposition of the first polyelectrolyte bilayer. Pt nanoparticles were subsequently adsorbed to the PEI layer during passage of 250 mL of the colloid solution (~0.02 mM in Pt atoms) prior to another rinse. Repetition of the PEI and Pt deposition process yielded additional bilayers. During the colloid adsorption, the fiber changed color from white to gray, indicating entrapment of Pt nanoparticles within the membrane.

2.4. Membrane Characterization. SEM images of hollow fibers before and after modification were obtained using a Hitachi S-4700 II field-emission scanning electron microscope (FESEM). Deposition of 8 nm of sputtered gold rendered the samples conductive for imaging. To prepare membrane cross sections, the fiber segments were soaked in ethanol for 2 min to completely wet the fiber before fracturing in liquid nitrogen and mounting for imaging. Because the Pt nanoparticle size is below the resolution of the FESEM, the Pt loading onto fibers was determined through analysis by inductively coupled plasma optical emission spectrometry (ICP-OES). Fibers were cut into several pieces, sonicated in aqua regia for 10 min, and these solutions were diluted prior to analysis with a Varian 710-ES ICP-OES at 214.424 nm.

2.5. Catalytic Reactions. Wet air oxidation of formic acid served as a model reaction for assessing the catalytic activity of PS hollow fibers. Initially, 250 mL of formic acid feed solution was pushed through the membrane in cross-flow at 0.34 bar to wet all pores. Again, a partially closed valve at the membrane outlet forced most of the flow from the lumen to the shell. Subsequently, a peristaltic pump pulled the formic acid solution through the fiber lumen at 0.1 mL/min while an O_2 or N_2 overpressure was applied to the shell side to prevent transmembrane flux. Four initial feed samples along with permeate samples at specified intervals were diluted and analyzed for formic acid

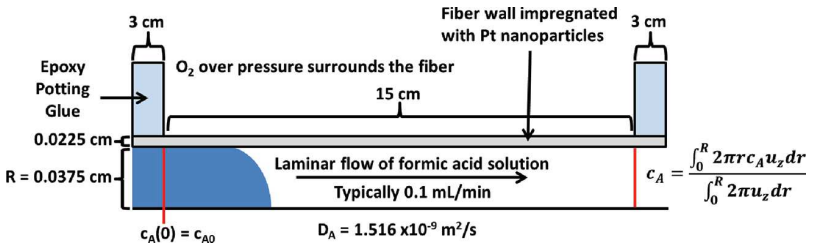

Figure 3. Modeled fiber system dimensions and boundary conditions for inlet and outlet formic acid concentrations showing only half of the lumen and a single wall.

using ion chromatography with a Dionex LC20 instrument equipped with an Ionpac AS16 column.

2.6. Modeling. The membrane reactor consists of a tubular fiber with solution introduced through the lumen, and the incoming formic acid reacts only in the fixed porous catalyst bed within the fiber walls. An overpressure on the shell side prevents transmembrane flow but is not sufficient to de-wet the pores. The model used for calculation couples the free fluid and porous media flow through the Navier-Stokes equations and Brinkman's extension of Darcy's law. Because of the symmetry of the system, only half of the fiber needs to be modeled using a 2D axisymmetric geometry. The Navier–Stokes equation describes the fluid flow in the lumen according to eq 1, where $\nabla u = 0$.

$$\nabla(-\eta(\nabla u + (\nabla u)^T + pI)) = -\rho(u\nabla)u \tag{1}$$

Within the porous wall, the Brinkman equation describes the flow according to eq 2, where $\nabla u = 0$. In these equations, η denotes the viscosity of

$$\nabla\left(-\frac{\eta}{\xi_p}(\nabla u + (\nabla u)^T + pI)\right) = -\frac{\eta}{k}u \tag{2}$$

the fluid (Ns/m^2), ε_p is the dimensionless porosity, u is the velocity (m/s), ρ is the density (kg/m^3), p is the pressure (Pa), κ is the permeability (m^2), and I is the identity matrix.

A Fickian approach is suitable for formic acid diffusion, and eq 3 provides the mole balance for formic acid mass transport and reaction.

$$\nabla(-D_A\nabla c_A + c_A u) = R_A \tag{3}$$

In eq 3, c_A denotes the concentration of formic acid (mol/m^3), D_A is the diffusivity (m^2/s), and R_A is the reaction rate for formic acid oxidation [mol/(m^3 s)]. We estimated D_A as 1.516×10^{-9} m^2/s.[58] The reaction only takes place in the porous walls, so the reaction term is zero in the lumen, and formic acid oxidation in the pores occurs according to eq 4.

$$HCOOH + \frac{1}{2}O_2 \rightarrow CO_2 + H_2O \tag{4}$$

Because the reaction rate did not vary significantly with external O_2 pressure within the range tested, we assumed a first-order reaction rate, $R_A = -kc_a$, where k is the reaction rate constant.

Upon the solution's entry into the lumen, a fully developed laminar flow is assumed and eq 5 gives the velocities

$$nu = u_{max}\left[1 - \left(\frac{r}{R}\right)^2\right] \tag{5}$$

where n is the boundary normal vector and r is the distance from thecenter of the circular cross-section with a total radius R. At the fiber outlet, the boundary conditions for the Navier-Stokes equations are $tu = 0$ and $p = 0$ where t is any tangential vector to the boundary. The formic acid concentration at the inlet was fixed as $c_A(0) = c_{A0}$. At the outlet, convection dominates the formic acid mass transport yielding $n(-D_A\nabla c_A + c_A u) = nc_A u$. This implies the gradient of c_A in the direction perpendicular to the outlet boundary is negligible, a common assumption for tubular reactors with a high degree of transport by convection in the direction of the main reactor axis (Figure 3). Thus, this condition eliminates the need for specifying a concentration or a fixed value for the flux at the outlet boundary. At all other boundaries, insulation conditions apply as given by eq 6.

$$n(-D_A\nabla c_A + c_A u) = 0 \tag{6}$$

Equation 7 describes the formic acid conversion where c_A is the mixing cup concentration at the outlet determined from eq 8. All calculations were performed in the chemical engineering module of COMSOL Multiphysics 3.5a.

$$x_A = \left(\frac{c_{A0} - c_A}{c_{A0}}\right) \tag{7}$$

$$c_A = \frac{\int_0^R 2\pi r c_A u_z dr}{\int_0^R 2\pi u_z dr} \tag{8}$$

3. RESULTS AND DISCUSSION

3.1. Membrane Modification with Pt Nanoparticles. Alternating adsorption of polyelectrolytes and Pt nanoparticles yields coated hollow fiber membranes with open pores. Adsorption occurs during permeation of polyelectrolyte or nanoparticle solutions from the lumen to the shell, so films deposit throughout the membrane wall, and the membrane turns gray after nanoparticle deposition. SEM images A and B in Figure 4 show no obvious changes in the membrane lumen

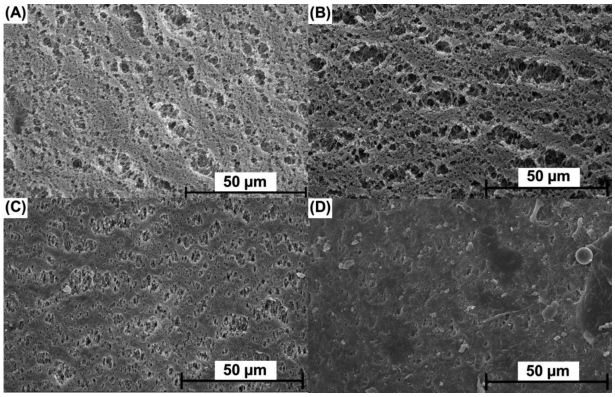

Figure 4. Representative SEM images of the (A, B) lumen and (C, D) shell surfaces of PS hollow fibers (A, C) before and (B, D) after adsorption of a PSS/(PEI/Pt nanoparticle)$_2$ film.

pore sizes after deposition of a PSS/[PEI/Pt]$_2$ film, presumably because the thickness of the polyelectrolyte/nanoparticle films is less than 10 nm.[38,59] Meanwhile, the images of the smaller pores on the shell side (Figure 4C, D) show some changes in the surface morphology after film deposition, but pores remain

Table 1. Pt Loading Per Length of Fiber after LBL Modification of a Single-Fiber Module and a Five-Fiber Module with PSS/$[PEI/Pt]_2$ Films[a]

	loading (μg Pt/cm)				
fiber	segment 1	segment 2	segment 3	segment 4	average
single	78.7 ± 3.5	76.8 ± 3.2	79 ± 2.0	80.9 ± 0.6	78.9 ± 2.6
			Five Fiber Module		
Fiber 1	38.8 ± 1.0	53.4 ± 0.8	44.6 ± 1.2	n/a	45.6 ± 0.9
Fiber 2	41.8 ± 0.6	56.9 ± 2.5	48.3 ± 0.7	n/a	49.0 ± 1.3
Fiber 3	36.9 ± 0.5	51.3 ± 0.5	31.1 ± 0.4	n/a	39.8 ± 0.4
Fiber 4	53.5 ± 1.1	58.7 ± 1.4	54.6 ± 0.6	n/a	55.6 ± 0.9
Fiber 5	47.4 ± 1.0	58.3 ± 0.8	47.9 ± 1.9	n/a	51.2 ± 1.2

[a]Loadings were determined by dissolution of the Pt in aqua regia and analysis by ICP-OES. The segments were approximately 3.75 cm long for the single fiber and 5 cm long for the 5-fiber module.

open. The absence of a cross-flow rinse on the shell side and solution dripping from this surface during modification likely leads to additional deposition on the shell compared to the lumen. When a cross-flow rinse was incorporated on the shell side during modification, no significant pore size reductions were visible in SEM images on either the lumen or shell surfaces. Overall, pore size reduction when depositing without crossflow decreased O_2 permeability <20% at 0.2 bar, so the open pores on the shell surface will afford the gaseous reactant access to the catalyst-solution interface.

To examine the uniformity of Pt loading along the length of a PS fiber modified with a PSS$[PEI/Pt]_2$ film, we cut a 15 cm long fiber into 3.75 cm long sections, dissolved the Pt in aqua regia, and analyzed the aqua regia solutions by ICP-OES. The relative standard deviation (RSD) in the Pt loading for the four segments (Table 1, row 1) was less than 10%. The uniform loading of Pt nanoparticles should ensure similar catalyst availability over the entire length of the fiber. We also simultaneously modified five fibers in a single module, cut each fiber into three 5 cm-long sections and determined the amount of Pt in each segment. In this case the relative standard deviation in the Pt content of the 15 segments was 17 % (Table 1, rows 2–6). Overall, the loading in the five-fiber module is about 60% of that in a single fiber. The lower deposition solution cross-flow rate during adsorption in the five-fiber module might lead to lower loadings.

3.2.1. Catalytic Performance of PS Hollow Fiber Modules. *CWAO of Formic Acid Using a Membrane Contactor.* Oxidation of formic acid is an ideal model reaction to test the catalytic activity of immobilized Pt nanoparticles because the only products are CO_2 and water, and Pt is a common catalyst for this reaction.[60−62] In a control experiment, we bubbled a 50 mM formic acid solution with O_2 and then passed this solution through the fiber lumen while applying a N_2 overpressure (0.69 bar) to the shell side of the membrane. One pass of the solution through a single Pt-modified PS hollow fiber at 0.1 mL/min (membrane residence time of 40 s) resulted in oxidation of only 6 ± 3 % of the formic acid (Figure 5, triangles). The low conversion stems from the limited O_2 solubility in the feed solution. The room-temperature solubility of O_2 in water is ~1.25 mM at 1 atm of O_2,[18,63] and one molecule of O_2 can oxidize two molecules of formic acid. Thus, the O_2 in solution can oxidize a maximum of ~2.5 mM formic acid, which is similar to the observed reaction of 6 ± 3 % of the 50 mM formic acid during passage through the membrane.

In contrast, application of an O_2 overpressure (0.69 bar) to the shell side of the hollow fiber resulted in steady-state oxidation of 63 ± 3 % of the formic acid in a 50 mM feed solution

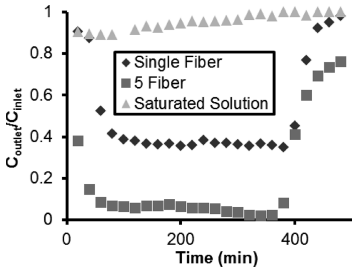

Figure 5. Ratio of the outlet to inlet concentrations of formic acid during CWAO in three different fiber modules coated with PSS/$[PEI/Pt]_2$ films. Triangles represent an O_2-saturated solution as the lone source of O_2 using a single Pt-coated PS fiber with N_2 (0.69 bar overpressure) on the shell side. Diamonds and squares represent a single and 5-fiber contactor reactor, respectively, where an O_2 overpressure (0.69 bar) was applied on the shell side at 0 min and subsequently replaced with a N_2 overpressure (0.69 bar) at 360 min. The solution flow rate was 0.1 mL/min in all cases.

during a single pass through the membrane lumen with a residence time of 40 s. (In this case, the solution was not saturated with O_2 prior to passing through the membrane.) As Figure 5 shows, after changing the gas in the module from 0.69 bar N_2 overpressure to 0.69 bar O_2 overpressure with no prior O_2 saturation of the feed, the concentration of formic acid exiting the membrane decreased to the steady state value of 37% of the feed concentration after displacing the dead volume (~4 mL) at the exit of the hollow fiber module, demonstrating the O_2 dependence of the reaction. After 360 min of oxidation, we changed the shell gas from 0.69 bar O_2 to 0.69 bar N_2 (overpressure), and conversion declined again confirming the importance of the membrane contactor for delivering O_2 to enhance conversion.

To increase the fraction of formic acid oxidized without decreasing the overall volumetric flow rate, we increased the number of fibers in the module. Notably, with modules containing 5 fibers, formic acid oxidation reaches 94 ± 3 % in a single pass (Figure 5, squares) without saturating the solution with O_2 prior to passing it through the membrane. The increase in conversion results from the higher residence times (198 s) in modules with more fibers. Further increases in the number of fibers will allow even higher conversions or similar conversions at higher flow rates through the module.

3.2.2. Fiber Longevity. The stability of modified fibers is a major concern because both oxidation of the polymer and shear stress may leach nanoparticles from the membrane. However, ten 8-hour replicates of CWAO (50 mM formic acid) with the

same fiber show a RSD in formic acid oxidation of less than 20%, suggesting no continuous leaching of Pt from the system (Figure 6). While there is some spread in the net conversions in

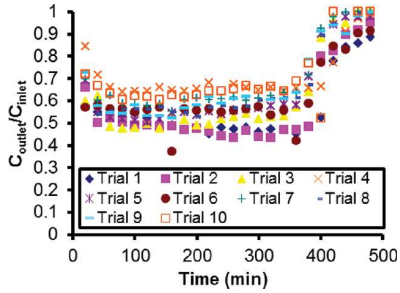

Figure 6. Ratio of the outlet to inlet concentrations of formic acid during CWAO for 10 trials of 8 h using a single PS fiber module modified with a PSS/$[PEI/Pt]_2$ film. An O_2 overpressure of 0.69 bar was applied at 0 min on the shell side and replaced with N_2 at 360 min.

different experiments, the general trends remain the same in every trial. More importantly, after the first three trials, no clear trend of decreasing conversion with each subsequent trial occurred. The conversion decline after the first three trials does not appear to result from Pt leaching because the conversion did not decrease significantly during the trials. Instead, an inactivation of some catalyst sites may occur during drying of the fiber between experiments. The outlying data points from trial six are probably the result of IC instrument error rather than increased performance. Therefore, the fiber remained relatively stable during the 80 hours of testing in this experiment.

3.2.3. Dependence of Oxidation Rates on Formic Acid Concentration and O_2 Overpressure. To explore the factors that limit the rate of CWAO in hollow fiber membranes, we varied both the formic acid concentration and the O_2 overpressure during reactions. Figure 7 shows the average concentration

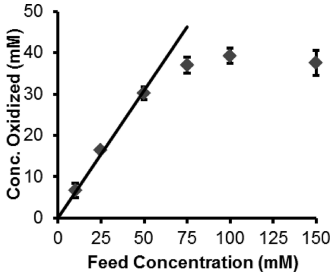

Figure 7. Concentration of formic acid oxidized (inlet−outlet concentration) in CWAO with a single-fiber module and an O_2 overpressure of 0.69 bar on the shell side of the membrane. The line represents a linear fit (forced through the origin, slope of 0.55) to the first three data points. Data are an average of multiple experiments with a single fiber.

of formic acid oxidized (the difference between feed and outlet concentrations) as a function of the formic acid concentration in the feed solution passed through a single-fiber module. Error bars represent the standard deviation of the average oxidized formic acid concentration over a period of 5 h. At feed concentrations from 10 to 50 mM, the change in formic acid concentration upon passing through the membrane varies approximately linearly with the feed concentration. In contrast, the concentration of formic acid oxidized in a single pass through the membrane plateaus at 40 mM for feed concentrations from 80 to 150 mM. These data suggest that formic acid concentration limits the reaction rate at low feed concentrations (due to either diffusion or kinetic limitations), whereas either the availability of O_2 in the catalyst layer or the amount of catalyst limit the reaction at high formic acid feed concentrations.

Figure 8 shows the average concentration of formic acid oxidized when using a 50 mM formic acid feed and various O_2

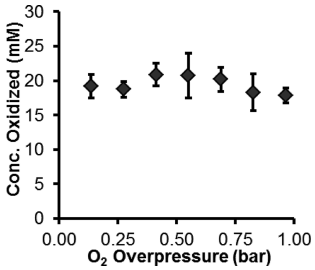

Figure 8. Concentration of formic acid oxidized during CWAO with single fiber modules at varying overpressures. Membranes were modified with PSS/$[PEI/Pt]_2$ films and the feed solution contained 50 mM formic acid. Data are an average of three replicate experiments with two different fibers.

overpressures on the shell side of single fiber modules. Within experimental error, the amount of formic acid oxidized is independent of the O_2 overpressure tested. The highest overpressure of ~1 bar represents the maximum recommended operating pressure from the manufacturer of this PS fiber. One concern in these experiments, however, is whether changing the overpressure alters the wetting of the pores. The Young−Laplace equation (eq 9),

$$\Delta p = \frac{2\gamma\cos(\theta)}{r} \tag{9}$$

provides an estimate for the critical pressure, Δp, required to prevent pore wetting, where θ is the solution contact angle with the material, γ is the surface tension of the liquid, and r is the pore radius. On the basis of a contact angle of 67° on polysulfone,[64] and a pore radius of 325 nm, this equation suggests that the pressure required to overcome capillary wetting would be around 1.7 bar for aqueous solutions. This is consistent with the fact that we observed no gas bubbles breaking through the membranes. If the pores are indeed wetted at all the pressures in these experiments, we would expect that increased O_2 solubility in water might enhance oxidation rates. The constant reaction rate at various O_2 pressures may stem from the narrow range of total pressures (1.1−2 bar absolute pressure) and the fairly complicated kinetics of the formic acid oxidation. Harmsen et al. suggest that an expression similar to eq 10 describes the rate of formic acid oxidation, R.[65]

$$R = \frac{K[O_2]^{1/2}[HCOO^-]}{(1 + K'[O_2]^{1/2} + K''[HCOO^-])^2} \tag{10}$$

In this expression, K, K', and K'' represent products of different equilibrium constants and surface site densities. At most, the reaction rate would show a square root dependence on the concentration of O_2 in solution.

3.2.4. Effect of Pt Loading on Conversion. Pt loading will limit the rate of formic acid oxidation when the catalyst is saturated with reactants. To examine the effect of catalyst loading

on oxidation rate, we compared single-fiber membrane reactors modified with one and three PEI/Pt bilayers atop a base layer of PSS. Analysis of Pt loading in these fibers using ICP-OES shows that adsorption of each PEI/Pt bilayer adds approximately 500 μg of Pt to the membrane. Figure 9 demonstrates

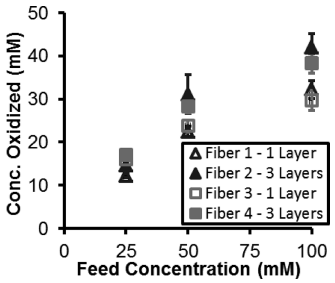

Figure 9. Concentration of formic acid oxidized (inlet−outlet concentration) in CWAO with a single-fiber module and various formic acid concentrations in the inlet solutions. Fibers 1 and 3 were replicate fibers modified with PSS/PEI/Pt (one-layer) films, whereas fibers 2 and 4 were modified with PSS[PEI/Pt]$_3$ (three-layer) films. The error bars in the figure represent standard deviations with an n value of more than 40.

that the amounts of formic acid oxidized in fibers containing 1 PEI/Pt bilayer (replicate fibers 1 and 3) are significantly less than in fibers containing 3 bilayers (replicate fibers 2 and 4) (p = 0.99) for feed solutions containing 50 and 100 mM formic acid. At feed concentrations of 25 mM, the two types of membranes show similar conversions, presumably because the catalyst is not saturated with reactant. As in Figure 5, the concentration oxidized increases with the feed (inlet) concentration. The average ratios of the concentrations oxidized in membranes modified with 3 and 1 PEI/Pt bilayers were 1.14, 1.28, and 1.31 at feed concentrations of 25, 50, and 100 mM, respectively. Thus, although higher Pt loading enhances formic acid oxidation, the increase of ~1.30 in the amount oxidized is significantly less than the 3-fold increase in Pt loading. Perhaps Pt in the inner layers of the coating is not effective in oxidation because of slow formic acid diffusion into the coating.

3.3. Calculated Formic Acid Concentration Profiles.

We first calculated the diffusion-limited formic acid conversion. In this calculation, we assumed laminar flow throughout the fiber lumen and that formic acid oxidation occurs instantaneously upon encountering the fiber wall, i.e, the concentration of formic acid at the lumen wall is zero. Figure 10 shows the resulting concentration profile. For a 15 cm long fiber and a flow rate of 0.1 mL/min, the mixing cup concentration exiting the fiber is only ~4% of the feed concentration (>96% oxidation of formic acid). Thus the reaction we observe in the fibers (40−60% oxidation) is significantly slower than the diffusion-limited case where reaction occurs instantaneously at the lumen wall. The diffusion-limited oxidation in the five-fiber module is even higher (>99.9%) because of the longer residence time, and this conversion is again much greater than the 94% we observed.

To more reasonably model the system, we allowed for diffusion to reaction sites within the membrane walls and varied the first-order rate constant for formic acid oxidation. We assumed fully developed laminar flow in the interior of the fiber and no convective flow in the membrane walls. Figure 11 shows the concentration profile in a single-fiber membrane reactor, assuming a rate constant within the fiber walls of 0.01 s^{-1}. The

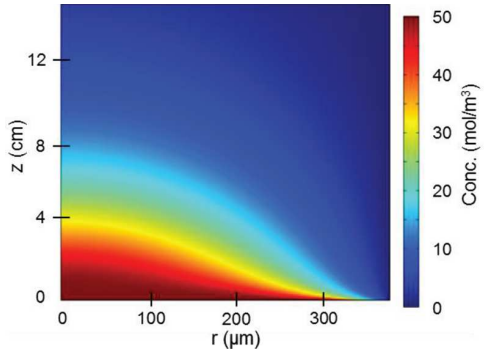

Figure 10. Diffusion-limited formic acid concentration profile in a single-fiber reactor as a function of the distances from the inlet (z, Y-axis) and the center of the fiber (r, X-axis). The fiber inner radius was 375 μm, and reaction was assumed to occur instantaneously at the fiber wall, where r = 375 μm. The results predict 96 % oxidation of the 50 mM formic acid by the time the solution reaches the outlet. The flow rate was 0.1 mL/min.

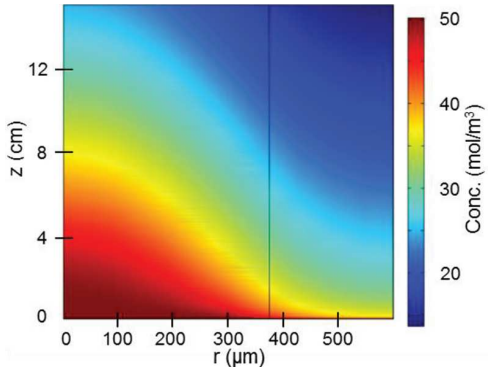

Figure 11. Calculated formic acid concentration profile during oxidation in a single-fiber reactor. The plot shows the concentration by color at any point along the length of the reactor (z, Y-axis) and at any radial distance between the center of the fiber to the outer wall (r, X-axis). The results predict ~52 % oxidation of the formic acid by the time the solution reaches the outlet. The assumed first-order rate constant was 0.01 s^{-1}.

vertical line indicates the lumen wall. In this case, a rate constant of 0.01 s leads to a formic acid concentration profile very different from that in the diffusion-limited case. Reaction occurs throughout the wall, but is more prevalent near the lumen. The mixing cup outlet concentration is about half that of the feed concentration, which agrees well with the observed conversion. Note that we assumed a first order rate constant because the O_2 pressure outside the fiber did not affect conversion, see Figure 7. In modeling the reaction in the five fiber module using the same rate constant, we also see agreement between experimental and observed conversion (94 ± 3 % experimental versus 97% in the simulation). Additionally, we modeled O_2 concentration profiles for the polymeric fiber module at overpressures of 0.1, 0.69, and 1 bar, see Figure S1 in the Supporting Information. As expected, the oxygen concentration decreases from the shell to the lumen, so a first-order reaction is an oversimplification. Near the lumen reaction rates will likely be lower than simulated, whereas near the shell wall they will be higher than simulated.

Figure 12 shows the predicted conversions for a single fiber module at a range of first-order rate constants from 0.001 to

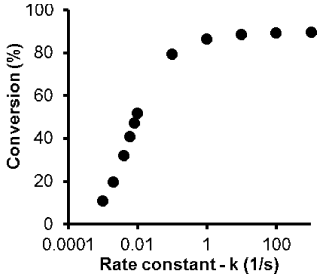

Figure 12. Calculated mixed cup conversion of formic acid for a single fiber reactor assuming first-order rate constants for formic acid wet air oxidation from .001 to 1000 s^{-1}.

1000 s^{-1}. At values above 1 s^{-1}, the reaction becomes limited by diffusion of formic acid to the walls of the fiber, and the concentration near the lumen wall is nearly zero. Rate constants below 0.01 s give much lower reaction than we observed. Conversion of the pseudo-homogeneous rate constant (k, 0.01 s^{-1}) to a heterogenous rate constant, k', requires normalization to the amount of Pt surface area, A, per solution volume, V, according to eq 11.

$$k' = \frac{kV}{A} \tag{11}$$

Given the total Pt loading of 1 mg in a single fiber and assuming 3 nm diameter particles, the value of k' is 8×10^{-7} cm/s.

Figure 13 shows the predicted effect of membrane wall thickness (over a range of 100-300 μm) on the extent of formic acid

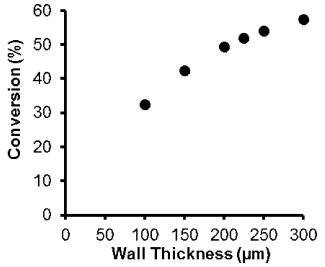

Figure 13. Calculated formic acid conversion in a single-fiber module with membranes having different wall thicknesses. The inner radius of the fiber was 375 μm, and the rate constant was 0.01 s^{-1}.

oxidation. We should note again that this calculation neglects any effect the wall thickness may have on the availability of O_2 for the reaction. The results suggest that the thickness of the wall plays a modest role in the oxidation process, as the extent of formic acid oxidation only increases from 32 to 57% on increasing the wall thickness from 100 μm to 300 μm. Most of the reaction takes place within the first 100 μm of the lumen surface. The model assumes that the pores of the membrane are completely wetted, which as mentioned above is likely given the size of the pores and the contact angle of the membrane.

3.4. Comparison to Previous Work. The best tubular ceramic membranes for CWAO in Miachon's work catalyzed oxidation of about 10% of a 100 mM formic acid solution during a single pass at a flow rate between 7 and 10 mL/min (linear velocity of 0.43 cm/s, residence time of 58 s, membrane length of 25 cm).[49] Those membranes had a lumen diameter of 7 mm, and our simulation of diffusion-limited oxidation in such large membranes gives a conversion of 13%, similar to the measured value (see Figure S2 in the Supporting Information). The innermost 3 μm layer of the lumen wall in the ceramic membranes contained 20 nm pores which likely allow a high Pt loading near this wall, as determined by SEM-EDS mapping.[2] The high catalyst loading at the lumen wall may lead to a rate that is closer to the diffusion limit than in the case of the hollow fiber membranes.

Nevertheless, at similar residence times, the polymer single fiber modules in this study give a higher single-pass conversion of formic acid than the previous ceramic hollow fibers, presumably because of the smaller average diffusion distances between the molecules in solution and the polymer fiber. (For the large fiber, the depletion layer around the lumen never reaches the center of the fiber, see Figure S2 in the Supporting Information.) Use of ceramic membranes with smaller lumen diameters (3 mm) should also reduce formic acid diffusion distances and lead to somewhat lower single-pass conversions. However, the cost of the ceramic membranes may still limit their practicality. Additionally, although smaller ceramic fibers still contain larger pores on the shell surface than the lumen, they may lack the distinct multilayered wall composition that afforded high catalyst density near the lumen surface in the work of Miachon.[66]

Remarkably, the five-fiber PS modules in this study catalyzed oxidation of 94% of the formic acid in a 50 mM feed solution in a single pass at a flow rate of 0.1 mL/min (linear velocity of 0.08 cm/s, residence time of 198 s, 15 cm fiber). Assuming performance remains the same with further scale up and the same linear velocity, a module containing 500 PS fibers would oxidize 94% of the formic acid in a single pass, whereas a single 7 mm (inside diameter) ceramic fiber would oxidize only about 10% of the formic acid at the same total flow rate. (The cost of a 500-fiber module is about the same as that of a ceramic fiber.)

One major disadvantage of the polymeric fibers, however, is the relatively low activity of the immobilized platinum. With a feed solution containing 100 mM formic acid, the modified PS fibers exhibited a normalized activity of 0.07 mmol formic acid/(s g Pt), whereas the best ceramic membranes showed an activity of 1.5 mmol formic acid/s g Pt). The higher activity in the ceramic membranes likely stems from the 3 layer geometry of the fibers, and the high concentration of catalyst near the lumen. Moreover, because outer pores do not wet, nearly all of the catalyst resides near the liquid–air interface to provide readily accessible O_2 for oxidation. In contrast, for the polymeric membrane Pt deposition and wetting occur throughout the fiber wall, so oxygen availability may significantly limit the reaction. Further refinement of catalyst deposition and wetting properties, probably using membranes with small pores at the lumen interface, should lead to increased activity in polymeric fiber reactors.

4. CONCLUSIONS

CWAO in single polymeric hollow fibers at room temperature leads to ~50% oxidation of the formic acid in 50 mM feed solutions during a single pass through a hollow fiber. Additionally, 94% oxidation occurs for a single pass through five parallel fibers at the same volumetric flow rate but lower linear velocity. The PS hollow fibers show significantly higher conversions than previous ceramic membranes because the small diameter of the hollow fibers decreases radial diffusion distances. Modeling the diffusion of formic acid within the lumen indicates the oxidation is significantly below the diffusion-limited rate. A simple first-order model of the reaction suggests an

apparent rate constant of 0.01 s^{-1} and shows that reaction occurs throughout the fiber wall.

One major challenge to the use of the catalytic PS hollow fibers is the low catalyst activity caused by a disperse loading of Pt nanoparticles throughout the wall of the fibers instead of in a tightly concentrated region near the lumen surface. With increased nanoparticle deposition localized near the lumen walls and more controlled pore wetting, the activity might improve without decreasing conversion.

ASSOCIATED CONTENT

Modeled formic acid concentration profile for a ceramic membrane with a diameter of 7 mm and a flow rate of 10 mL/min, and simulated O_2 concentration profiles in a hollow fiber module at overpressures of 0.1, 0.69, and 1.0 bar. This material is available free of charge via the Internet at http://pubs.acs.org.

AUTHOR INFORMATION

Corresponding Author

*Phone: +1-517-355-9715, ×237. Fax: +1-517-353-1793. E-mail: bruening@chemistry.msu.edu.

Notes

The authors declare no competing financial interest.

ACKNOWLEDGMENTS

We thank the National Science Foundation (OIS 0530174) for funding this research.

REFERENCES

(1) Besson, M.; Descorme, C.; Bernardi, M.; Gallezot, P.; di Gregorio, F.; Grosjean, N.; Pham Minh, D.; Pintar, A. *Environ. Technol.* **2010**, *31*, 1441.
(2) Vospernik, M.; Pintar, A.; Berčič, G.; Levec, J.; Walmsley, J. C.; Ræder, H.; Iojoiu, E. E.; Miachon, S.; Dalmon, J.-A. *Chem. Eng. Sci.* **2004**, *59*, 5363.
(3) Fritsch, D.; Bengtson, G. *Adv. Eng. Mater.* **2006**, *8*, 386.
(4) Gabelman, A.; Hwang, S.-T. *J. Membr. Sci.* **1999**, *159*, 61.
(5) Miachon, S.; Perez, V.; Crehan, G.; Torp, E.; Ræder, H.; Bredesen, R.; Dalmon, J.-A. *Catal. Today* **2003**, *82*, 75.
(6) Westermann, T.; Melin, T. *Chem. Eng. Process.* **2009**, *48*, 17.
(7) Kleinert, A.; Feldhoff, A.; Schiestel, T.; Caro, J. *Catal. Today* **2006**, *118*, 44.
(8) Peters, T. A.; Fontalvo, J.; Vorstman, M. A. G.; Keurentjes, J. T. F. *Chem. Eng. Res. Des.* **2004**, *82*, 220.
(9) Wang, H.; Tablet, C.; Schiestel, T.; Caro, J. *Catal. Commun.* **2006**, *7*, 907.
(10) Mulder, M. *Basic Principles of Membrane Technology*; Kluwer Academic Publishers: Dordrecht, The Nethelands, 1996.
(11) Ouyang, L.; Dotzauer, D. M.; Hogg, S. R.; Macanas, J.; Lahitte, J.; Bruening, M. *Catal. Today* **2010**, *156*, 100.
(12) Wang, H.; Feldhoff, A.; Caro, J.; Schiestel, T.; Werth, S. *AIChE J.* **2009**, *55*, 2657.
(13) Van der Vaart, R.; Lebedeva, V. I.; Petrova, I. V.; Plyasova, L. M.; Rudina, N. A.; Kochubey, G. F.; Tereshchenko, G. F.; Volkov, V. V.; van Erkel, J. *J. Membr. Sci.* **2007**, *299*, 38.
(14) Peirano, F.; Vincent, T.; Quignard, F.; Robitzer, M.; Guibal, E. *J. Membr. Sci.* **2009**, *329*, 30.
(15) Blondet, F. P.; Vincent, T.; Guibal, E. *Int. J. Biol. Macromol.* **2008**, *43*, 69.
(16) Israni, S. H.; Nair, B. K. R.; Harold, M. P. *Catal. Today* **2009**, *139*, 299.
(17) Caro, J.; Caspary, K. J.; Hamel, C.; Hoting, B.; Kolsch, P.; Langanke, B.; Nassauer, K.; Schiestel, T.; Schmidt, A.; Schomacker, R.; Seidel-Morgenstern, A.; Tsotsas, E.; Voigt, I.; Wang, H.; Warsitz, R.; Werth, S.; Wolf, A. *Ind. Eng. Chem. Res.* **2007**, *46*, 2286.
(18) Dotzauer, D. M.; Abusaloua, A.; Miachon, S.; Dalmon, J.-A.; Bruening, M. L. *Appl. Catal., B* **2009**, *91*, 180.
(19) Astruc, D.; Lu, F.; Aranzaes, J. R. *Angew. Chem., Int. Ed.* **2005**, *44*, 7852.
(20) Pool, R. *Science* **1990**, *248*, 1186.
(21) Mei, Y.; Sharma, G.; Lu, Y.; Ballauff, M.; Drechsler, M.; Irrgang, T.; Kempe, R. *Langmuir* **2005**, *21*, 12229.
(22) Comotti, M.; Li, W. C.; Spliethoff, B.; Schüth, F. *J. Am. Chem. Soc.* **2006**, *128*, 917.
(23) Jiang, Y.; Gao, Q. *J. Am. Chem. Soc.* **2006**, *128*, 716.
(24) Meyer, D. E.; Bhattacharyya, D. *J. Phys. Chem. B* **2007**, *111*, 7142.
(25) Brandão, L.; Fritsch, D.; Mendes, A. M.; Madeira, L. M. *Ind. Eng. Chem. Res.* **2007**, *46*, 5278.
(26) Valden, M.; Lai, X.; Goodman, D. W. *Science* **1998**, *281*, 1647.
(27) Park, K. H.; Jang, K.; Kim, H. J.; Son, S. U. *Angew. Chem., Int. Ed.* **2007**, *46*, 1152.
(28) Pachón, L. D.; Rothenberg, G. *Appl. Organomet. Chem.* **2008**, *22*, 288.
(29) Bhattacharjee, S.; Dotzauer, D. M.; Bruening, M. L. *J. Am. Chem. Soc.* **2009**, *131*, 3601.
(30) Perez, V.; Miachon, S.; Dalmon, J. A.; Bredesen, R.; Pettersen, G.; Ræder, H.; Simon, C. *Sep. Purif. Technol.* **2001**, *25*, 33.
(31) Zhong, L. S.; Hu, J. S.; Cui, Z. M.; Wan, L. J.; Song, W. G. *Chem. Mater.* **2007**, *19*, 4557.
(32) Gates, B. C. *Chem. Rev.* **1995**, *95*, 511.
(33) Wolf, A.; Schüth, F. *Appl. Catal., A* **2002**, *226*, 1.
(34) Zheng, N.; Stucky, G. D. *J. Am. Chem. Soc.* **2006**, *128*, 14278.
(35) Dotzauer, D. M.; Bhattacharjee, S.; Wen, Y.; Bruening, M. L. *Langmuir* **2009**, *25*, 1865.
(36) Dotzauer, D. M.; Dai, J.; Sun, L.; Bruening, M. L. *Nano Lett.* **2006**, *6*, 2268.
(37) Bhattacharjee, S.; Bruening, M. *Langmuir* **2008**, *24*, 2916.
(38) Kidambi, S.; Bruening, M. L. *Chem. Mater.* **2005**, *17*, 301.
(39) Cho, J.; Caruso, F. *Chem. Mater.* **2005**, *17*, 4547.
(40) Ostrander, J. W.; Mamedov, A. A.; Kotov, N. A. *J. Am. Chem. Soc.* **2001**, *123*, 1101.
(41) Kidambi, S.; Dai, J.; Li, J.; Bruening, M. L. *J. Am. Chem. Soc.* **2004**, *126*, 2658.
(42) Jiang, C.; Markutsya, S.; Tsukruk, V. V. *Langmuir* **2004**, *20*, 882.
(43) Joly, S.; Kane, R.; Radzilowski, L.; Wang, T.; Wu, A.; Cohen, R. E.; Thomas, E. L.; Rubner, M. F. *Langmuir* **2000**, *16*, 1354.
(44) Caruso, F.; Caruso, R. A.; Möhwald, H. *Science* **1998**, *282*, 1111.
(45) Datta, S.; Cecil, C.; Bhattacharyya, D. *Ind. Eng. Chem. Res.* **2008**, *47*, 4586.
(46) Schönhoff, M. *J. Phys.: Condens. Matter* **2003**, *15*, R1781.
(47) Gheith, M. K.; Sinani, V. A.; Wicksted, J. P.; Matts, R. L.; Kotov, N. A. *Adv. Mater.* **2005**, *17*, 2663.
(48) Iojoiu, E. E.; Landrivon, E.; Ræder, H.; Torp, E. G.; Miachon, S.; Dalmon, J.-A. *Catal. Today* **2006**, *118*, 246.
(49) Iojoiu, E. E.; Miachon, S.; Landrivon, E.; Walmsley, J. C.; Ræder, H.; Dalmon, J.-A. *Appl. Catal., B* **2007**, *69*, 196.
(50) Ræder, H.; Bredesen, R.; Crehan, G.; Miachon, S.; Dalmon, J.-A.; Pintar, A.; Levec, J.; Torp, E. *Sep. Purif. Technol.* **2003**, *32*, 349.
(51) Iojoiu, E. E.; Walmsley, J. C.; Ræder, H.; Miachon, S.; Dalmon, J.-A. *Catal. Today* **2005**, *104*, 329.
(52) Iojoiu, E. E.; Miachon, S.; Dalmon, J.-A. *Top. Catal* **2005**, *33*, 135.
(53) Dalmon, J.-A.; Cruz-Lopez, A.; Farrusseng, D.; Guilhaume, N.; Iojoiu, E. E.; Jalibert, J.-C.; Miachon, S.; Mirodatos, C.; Pantazidis, A.; Rebeilleau-Dassonneville, M.; Schuurman, Y.; van Veen, A. C. *Appl. Catal., A* **2007**, *325*, 198.
(54) Brugger, P. A.; Cuendet, P.; Gratzel, M. *J. Am. Chem. Soc.* **1981**, *103*, 2923.
(55) Rouaix, S. C., C.; Aimar, P. *J. Membr. Sci.* **2006**, *277*, 137.
(56) Malaisamy, R.; Bruening, M. L. *Langmuir* **2005**, *21*, 10587.
(57) Kotov, N. A. *Nanostruct. Mater.* **1999**, *12*, 789.

(58) Bidstrup, D. E.; Geankoplis, C. J. *J. Chem. Eng. Data* **1963**, *8*, 170.
(59) Harris, J. J.; Bruening, M. L. *Langmuir* **2000**, *16*, 2006.
(60) Fein, D. E.; Wachs, I. E. *J. Catal.* **2002**, *210*, 241.
(61) Palaikis, L.; Wieckowski, A. *Catal. Lett.* **1989**, *3*, 143.
(62) Fonseca, I.; Jiang, L.; Pletcher, D. *J. Electrochem. Soc.* **1983**, *130*, 2187.
(63) *IUPAC Solubility Data Series Vol. 7: Oxygen and Ozone*; Battino, R., Ed.; Pergamon Press: New York, 1981; Vol. 7.
(64) Kim, K. S.; Lee, K. H.; Cho, K.; Park, C. E. *J. Membr. Sci.* **2002**, *199*, 135.
(65) Harmsen, J. M. A.; Jelemensky, L.; Van ANdel-Scheffer, P. J. M.; Kuster, B. F. M.; Marin, G. B. *Appl. Catal., A* **1997**, *165*, 499.
(66) Dutczaka, S. M.; Luiten-Oliemanb, M. W. J.; Zwijnenbergc, H. J.; Bolhuis-Versteegd, L. A. M.; Winnubstb, L.; Hempeniuse, M. A.; Benesa, N. A.; Wessling, M.; Stamatialisd, D. *J. Membr. Sci.* **2011**, *372*, 182.